Biomaterials 115 (2017) 19–29

Contents lists available at ScienceDirect

Biomaterials

journal homepage: www.elsevier.com/locate/biomaterials

A novel 3D in vitro metastasis model elucidates differential invasive strategies during and after breaching basement membrane

Asja Guzman, Víctor Sánchez Alemany, Yen Nguyen, Catherine Ruiqi Zhang, Laura J. Kaufman*

Columbia University, Department of Chemistry, New York, NY 10027, United States

ARTICLE INFO

Article history:
Received 24 September 2016
Received in revised form
8 November 2016
Accepted 14 November 2016
Available online 15 November 2016

Keywords:
Metastasis
Spheroid
Collagen
Invasion
Model system
Cancer

ABSTRACT

Invasive breast cancer and other tumors of epithelial origin must breach a layer of basement membrane (BM) that surrounds the primary tumor before invading into the adjacent extracellular matrix. To analyze invasive strategies of breast cancer cells during BM breaching and subsequent invasion into a collagen I-rich extracellular matrix (ECM), we developed a physiologically relevant 3D in vitro model that recreates the architecture of a solid tumor with an intact, degradable, cell-assembled BM layer embedded in a collagen I environment. Using this model we demonstrate that while the BM layer fully prevents dissemination of non-malignant cells, cancer cells are capable of breaching it and invading into the surrounding collagen, indicating that the developed system recreates a hallmark of invasive disease. We demonstrate that cancer cells exhibiting individual invasion in collagen matrices preferentially adopt a specific mode of collective invasion when transmigrating a cell-assembled BM that is not observed in any other tested fibrillar, non-fibrillar, or composite ECM. Matrix-degrading enzymes are found to be crucial during BM breaching but not during subsequent invasion in the collagen matrix. It is further shown that multicellular transmigration of the BM is less susceptible to pharmacological MMP inhibition than multicellular invasion in composite collagen/basement membrane extract matrices. The newly developed in vitro model of metastasis allows 3D cancer cell invasion to be studied not only as a function of a particular tumor's genetics but also as a function of its heterogeneous environment and the different stages of invasion. As such, this model is a valuable new tool with which to dissect basic mechanisms of invasion and metastasis and develop new therapeutic approaches in a physiologically relevant, yet inexpensive and highly tunable, in vitro setting.

1. Introduction

Breast cancer deaths occur primarily from metastatic disease that compromises function of critical organs. In carcinomas (epithelium-derived cancers), the most common type of breast cancer, metastasis requires tumor cells to breach the basement membrane (BM), a subtype of extracellular matrix (ECM) that surrounds the primary tumor, invade collagen I- and fat-rich ECM of the adjacent soft tissue, and intravasate into blood or lymph vessels where they will be transported to distant sites [1]. While a complex interplay of genetic and epigenetic changes underlies the multi-step metastatic cascade, dynamic interactions between tumor cells and the ECM are increasingly recognized as a key aspect of metastatic progression [2,3].

The BM is a specialized cell-adherent ECM produced jointly by normal and/or pathological epithelial, endothelial, and stromal cells. It is formed in a multi-step process initiated by cells binding laminin at the cell surface and subsequent accumulation of the non-fibrillar collagen IV at the nascent laminin scaffold. This process leads to a dense sheet-like matrix that under normal circumstances separates the epithelium or endothelium from the adjacent stroma [4,5]. BM deposition and turnover are often perturbed in cancers, resulting in matrices that are less crosslinked and thus more accessible to degradation and remodeling [4,6,7]. Discontinuities of BM surrounding primary tumors are caused by altered expression and crosslinking of BM components as well as enhanced enzymatic degradation, all hallmarks of aggressive cancers and each of established prognostic value [8–12].

In contrast to the non-fibrillar BM, stromal ECM in most organs

* Corresponding author.
E-mail address: kaufman@chem.columbia.edu (L.J. Kaufman).

http://dx.doi.org/10.1016/j.biomaterials.2016.11.014
0142-9612/

and connective tissues is dominated by collagen I, a fibrillar collagen [13]. The stromal ECM also displays abnormalities in composition and organization during carcinogenesis, which lead to changes in biomechanical properties and matrix architecture. The high breast tissue density associated with poor prognosis in patients with breast cancer is due in part to enhanced deposition of mostly fibrillar collagens [14–18]. Moreover, highly linearized and aligned collagen at tumor boundaries has been found to contribute to tumor invasion and linked to poor prognosis [19,20].

At the molecular level, cancer progression and metastasis have long been associated with the epithelial-mesenchymal transition (EMT). This process includes aberrant activation of transcription factors, altered expression and reorganization of cell surface and cytoskeletal proteins, and production of ECM-degrading enzymes, together resulting in a pro-migratory cellular phenotype [21,22]. The contribution of BM/ECM biomechanics to tumor progression has also been recognized, and several studies have reported stiffness-driven induction of EMT [23,24] and dramatic changes in invasive behavior in response to matrix stiffness and architecture [25–27].

Still, the cellular processes that lead to and occur alongside tumor cells traversing the BM layer and entering the surrounding ECM as invasive entities are insufficiently understood. This incomplete understanding is caused in part by the considerable difficulties of studying these processes in vivo and in vitro. In vivo, studies are hindered by limitations related to microscopic observations at the tumor site including imaging depth, resolution and overall imaging quality degraded by light scattering and physiological motion [28,29]. In contrast, while in vitro approaches offer good optical accessibility, they often use models of limited physiological relevance. Such in vitro studies typically rely on either 2D models, which do not recapitulate the dimensionality and biomechanics of the tumor microenvironment, or cells seeded in 3D matrices that do not mimic the tumor architecture or the heterogeneous nature of the tumor environment at the BM/ECM interface. While studies employing multicellular tumor spheroids (MTSs or spheroids) embedded in biopolymer matrices overcome some of these issues and represent a good model for cancer cell invasion in soft tissue [30], they do not recapitulate the initial invasive events, namely transmigration of the BM. Indeed, there are very few studies that address cancer cells consecutively migrating through BM and invading into stromal ECM as occurs in vivo [31,32].

Here we present a novel, biochemically well-defined and optically accessible 3D in vitro model for analysis of tumor cells during BM breaching and subsequent invasion into collagen I-rich environments. The newly established protocol allows spheroids to be surrounded with a BM layer of tunable thickness that consists of exogenously added BM components bound and assembled into a scaffold in a cell-mediated process. These “shelled” spheroids may then be embedded in 3D collagen matrices of variable biomechanical properties for extended culture and monitoring. Using this new model, we demonstrate that the presence of a BM layer is sufficient to induce a switch from individual to multicellular invasion, thus recapitulating a fundamental feature of the metastatic process in vivo. This new model allows tumor cell invasion to be investigated not only as a function of the distinct genetic characteristics of the tumor cells but also as a function of a tumor's heterogeneous environment and the different stages of invasion, thus offering a new tool for delineating basic mechanisms of invasion and developing new therapeutic approaches in a physiologically relevant setting.

2. Materials and methods

2.1. Cell lines and reagents

MDA-MB468 (referred to as MB468) breast cancer cells were obtained from the American Type Culture Collection (Manassas, VA). MCF10A and MCF10A-HRas cells were a gift from Professor Carol Prives (Columbia University, NY). All cell culture reagents unless otherwise stated were obtained from Gibco (Grand Island, NY). Ultra-low attachment plates were obtained from NOF American Corporation (Lipidure microplates) (Irvine, CA) or from Thermo Fisher Scientific (Nunclon Sphera microplates, pre-treated with 2% bovine serum albumin (BSA) to block protein absorption to plate surface) (Waltham, MA). Pepsin-treated (PT) bovine collagen I was obtained from Advanced BioMatrix (San Diego, CA) as a 5.9–6.1 mg/ml solution. Growth factor-reduced, phenol red-free basement membrane extract (BME)/Matrigel was obtained as an 8.9–10 mg/ml solution from BD Biosciences (San Jose, CA). Fluorescein-conjugated DQ type IV collagen was obtained from Life Technologies (Carlsbad, CA), dissolved in distilled, deionized H_2O (ddH_2O) and used as a 1 mg/ml solution. HiLite488-conjugated laminin was obtained from Cytoskeleton Inc. (Denver, CO), dissolved in ddH_2O and used as a 1 mg/ml solution. 10× DMEM solution, sterile NaOH (1 N) and sodium bicarbonate solution (7.5%) were purchased from Sigma-Aldrich (St. Louis, MO). Gibco 4-(2-hydroxyethyl)-1-piperazineethanesulfonic acid (HEPES) buffer (1 M) was obtained from Invitrogen (Carlsbad, CA). Protease inhibitor cocktail (P1860) was obtained from Sigma-Aldrich. Triton-X and marimastat (BB-2516) were obtained from EMD Millipore Chemicals (Billerica, MA). 10% buffered formalin phosphate was obtained from Fisher Scientific (Pittsburgh, PA). AlexaFluor-conjugated phalloidin was obtained from Invitrogen Life Technologies (Grand Island, NY). Fluorescent carboxy-modified microspheres (FluoSpheres 1 μm, $\lambda_{ex/em}$ = 535/575 nm, 2% solids) were obtained from Thermo Fisher Scientific.

2.2. Cell culture

MCF10A and MCF10A-HRas cells were cultured in 1× DMEM/F-12 medium supplemented with 5% (v/v) horse serum, 1% (v/v) 100× penicillin/streptomycin/amphotericin B solution (MP Biomedicals, Solon, OH), 0.5 μg/ml hydrocortisone (Sigma-Aldrich), 10 μg/ml insulin (Sigma-Aldrich), 0.1 μg/ml cholera toxin (Sigma-Aldrich) and 20 ng/ml EGF (Sigma-Aldrich) at 37 °C with 5% carbon dioxide. MB468 cells were cultured in 1× high glucose DMEM medium supplemented with 10% (v/v) fetal bovine serum, 1% (v/v) 100× penicillin/streptomycin/amphotericin B solution and 1% (v/v) 100× non-essential amino acids solution at 37 °C with 5% carbon dioxide. All cells were sub-cultured when 70–80% confluent.

2.3. Generation of multicellular tumor spheroids

Shell-free spheroids were formed using a centrifugation method described previously [33]. In brief, cells were brought into suspension in culture medium containing 0.2575 mg/ml BME and centrifuged at 4 °C for 10 min at 1000–1200 g in a Sorvall desktop centrifuge in ultra-low adhesion U-bottom culture plates. Culture plates were then transferred to an incubator for 24 h at 37 °C with 5% carbon dioxide, allowing spheroid compaction. Spheroids were then treated with Cell Recovery Solution (Corning, Corning, NY) for 45–75 min at 4 °C (time depending on cell type) prior to embedding in 3D matrices.

Prior to treatment with Cell Recovery Solution, a non-enzymatic mild chaotropic agent, spheroids prepared as described above had a layer of BME of variable thickness, density, and continuity, making them unsuitable for study of cells breaching BM. Thus, a variation of this method was developed to prepare fully shelled spheroids. To prepare spheroids surrounded by a continuous BM layer, cells were brought into suspension in ice-cold culture medium containing 0.2575 mg/ml total extracellular matrix proteins, consisting of

0.2500–0.2565 mg/ml BME and 0.0010–0.0075 mg/ml collagen type IV. Care was taken to ensure uniform distribution of BME and collagen IV in the solution, and perturbation of the solution after pipetting it into the culture plates was kept to a minimum. For formation of spheroids uniformly surrounded with a continuous BM, preventing adsorption of soluble matrix proteins onto the substrate was found to be critical. As such, Lipidure- or Nunclon Sphera-coated U-bottom 96-well plates additionally blocked with BSA were used. Centrifugation and transfer to the incubator was performed as described above for shell-free spheroids. Perturbation during transfer to the incubator was also kept to a minimum to prevent formation of irregularly shaped cell aggregates. Spheroid and shell were allowed to form for 24 h under standard cell culture conditions. For preparation of fluorescently labeled spheroids, adherent cells were incubated with Vybrant DiD cell labeling solution (Thermo Fischer Scientific), diluted 1:200 in growth medium for 1 h at 37 °C, rinsed twice with PBS and processed as described in the spheroid preparation protocol above.

2.4. Preparation of hydrogel-embedded spheroids

Spheroids with or without a BM shell were prepared as described in the section above. Single spheroids were placed into one of three types of biopolymer solution (collagen I, BME, or composite collagen I/BME), each of which could then be gelled around the spheroid. Spheroids without a BM shell were placed in the solution directly after treatment with Cell Recovery Solution. Spheroids with a BM shell were washed with pre-warmed PBS 5 min at room temperature to remove loosely bound BM and debris before placement into the solution. Collagen I solutions at 1 mg/ml were prepared by diluting a high-concentration collagen stock solution. Appropriate amounts of collagen stock solution were prepared with 10% (v/v) 10× DMEM, 2.5% (v/v) HEPES buffer, 2.5% (v/v) sodium bicarbonate and ddH_2O. All solutions were held and mixed at 4 °C. NaOH was added to adjust the pH to 7.4, and 200 μl of the neutralized collagen solution was immediately added to a chamber consisting of a 5 mm glass cylinder glued to a coverslip-bottom cell culture dish. A nylon mesh was placed on the inner circumference of the cylinder to anchor the gel. A single spheroid in 5 μl liquid was added to the liquid collagen. The gel chamber was then transferred to the 37 °C incubator. The collagen gels were overlaid with 50 μl growth medium after completion of gelation (t = 1 h) and surrounded by 700–1000 μl medium to prevent drying during extended monitoring following the incubation period. To prepare BME matrices loaded with a single spheroid, BME stock solution (8.9–10 mg/ml) was diluted with ice cold 1× DMEM to the final concentration of 3 mg/ml, 200 μl of the solution was added to a gel chamber and a single spheroid was added as described above. All steps were performed at 4 °C with pre-chilled solutions and instruments and transferred immediately to the 37 °C incubator. The gels were overlaid and surrounded with growth medium after 1 h as described above. For composite collagen I/BME gels, first 10× DMEM, HEPES buffer, and sodium bicarbonate were mixed. Then, the required amount of BME stock solution was added to reach the final concentration of 3 mg/ml. The BME replaced a proportion of the ddH_2O that would be added in the equivalent pure collagen gel. Subsequently the collagen stock solution was added to achieve a concentration of 1 mg/ml, and the solution was brought to pH 7.4 by adding NaOH. After careful mixing, the solution was transferred to the chamber, a single spheroid was added and gelation and liquid overlay was performed as described above.

2.5. Cell treatments

Inhibition of endogenous proteases for cells cultured in 3D environments was achieved through addition of the following agents (as described in Ref. [34]): aprotinin (targets serine proteases), bestatin (targets aminopeptidases), E-64 (targets cysteine proteases), leupeptin (targets serine and cysteine proteases), pepstatin: (targets acid proteases) and marimastat (targets MMP-1, -2, -3, -7, -9 and -14 (MT1-MMP)). All inhibitors except marimastat were contained in the P1860 inhibitor cocktail (Sigma-Aldrich), which was supplemented with 100 μM marimastat. The MMP inhibitors were dissolved in DMSO, which was used as solvent control in all MMP inhibition experiments.

Spheroids were pre-treated with inhibitors or the respective solvent control diluted in growth medium for 2 h at 37 °C in ultra-low adhesion plates before Cell Recovery Solution treatment (for spheroids without BM) and before washing steps (for spheroids with a BM layer). Both the collagen solution and the growth medium added on top of the 3D collagen matrix were supplemented with inhibitors at the same concentration as the pre-treatment solution.

2.6. Microscopy

Spheroids and individual cells in 3D matrices were imaged with a 10× (NA = 0.4) air and/or 60× (NA = 1.42) oil objective on an inverted confocal laser-scanning microscope (Olympus Fluoview 300) in either scanning transmittance, confocal reflectance, or confocal fluorescence mode. An Argon ion laser at 488 nm was used for excitation of fluorescein and HiLite488a and a Helium-Neon laser at 543 nm was used for excitation of AlexaFluor568. Fluorescence was detected on photo-multiplier tube detectors (PMT). Unlabeled collagen I was imaged via confocal reflectance microscopy (CRM) with the 60× oil objective using the 488 nm laser for excitation and a PMT for detection. Live cell imaging was performed using a custom-built microscope incubation chamber and objective heater to keep cells at 37 °C and 5% CO_2.

2.7. Quantification of imaging data

For quantitative assessment of invasion, spheroids were imaged in transmittance mode at 2 h and 24 h after implantation, with particular number of spheroids assessed noted in the figure captions. From the 10× magnification spheroid images, invasive area for each spheroid was determined. Invasive area was defined as the difference between the area of the 2D projection of the spheroid at t = 2 h and t = 24 h. In cases with extensive individual cell invasion – as observed for spheroids without BM shells in pure collagen matrices – a circle was used to quantify invasive area (Fig. S1a). In cases with primarily collective invasion, as observed for spheroids without BM shells in composite collagen/BME matrices, invasive multicellular strand boundaries were traced, and the area of the resulting shape was used for further calculations (Fig. S1b). To assess the significance of differences observed between groups of $5 < n < 20$, the non-parametrical Mann-Whitney-Wilcoxon test was applied as described in Ref. [35].

3. Results

To investigate cellular migratory behavior during the initial steps of invasion under physiologically relevant and biochemically defined conditions, we developed and used a novel experimental model for multicellular cancer cell invasion that allows monitoring cancer cells breaching a cell-bound basement membrane and subsequently invading into a three-dimensional collagen-rich matrix.

We have previously addressed breast cancer invasion using multicellular tumor spheroids embedded in 3D collagen, BME, or

collagen/BME composite matrices [27,36]. While these matrices represent appropriate models for cancer cell invasion in soft tissue, spheroid invasion into such environments does not recapitulate the serial nature of invasion in vivo, which requires breaching of BM before dissemination into stromal ECM. Thus, we developed a protocol for surrounding spheroids with a BM layer of tunable thickness and subsequently implanting those shelled spheroids into 3D biopolymer matrices in which BM transmigration and ECM invasion can be monitored (Fig. 1).

To assess the size of the BM layer and its integrity over time, BM-shelled spheroids were embedded into 1 mg/ml collagen I gels loaded with 1 μm fluorescent beads. These beads are smaller than the pores of the collagen I matrix but larger than those in the BM layer and are thus excluded from that layer. Confocal fluorescence microscopy (CFM) of an MB468 spheroid prepared with a BM shell showed a roughly circular area significantly larger than the spheroid from which beads were excluded (Fig. 2a). Imaging over the height of the spheroid indicated that the BM layer enveloped the spheroid (Video S1). While the spheroid was shielded from the bead-loaded collagen I initially, sites of bead accumulation at and within the spheroid could be observed 24 h after embedding, suggesting that the BM layer was partially degraded and the tumor cells were interacting with the surrounding, bead-loaded collagen I matrix (Fig. 2b).

To more fully establish whether the BM shell prevents the spheroid from direct contact with the collagen I matrix, spheroids with a BM shell were implanted into collagen I matrices and subjected to confocal reflectance microscopy (CRM), which allows visualization of unlabeled collagen fibers but not of non-fibrillar substrates such as BM. Indeed, the spheroids with BM shells displayed an area beyond the spheroid periphery devoid of collagen fibers, and the collagen fibers closest to the spheroids were isotropically arranged (Fig. 2c). This was in contrast to spheroids without a shell, which had collagen fibers adjacent to the spheroid surface that were radially aligned, indicating traction generation by cells in the spheroid (Fig. S2). Once the BM shell was breached and cells had established direct contact with the collagen matrix, radially aligned collagen fibers at the spheroid surface of initially shelled spheroids were also apparent (Fig. 2d).

We next addressed whether formation of the BM layer resembles the process in vivo, relying on laminin for the initial scaffold and collagen IV as a central structural component [4]. To this end, fluorescently labeled laminin or type IV collagen was introduced into the media during spheroid formation, reducing the amount of unlabeled BM proteins accordingly to keep the total concentration of exogenous BM components constant. Accumulation of fluorescent material around the spheroid was analyzed using CFM 2 h after implanting the spheroids in the surrounding gel. Laminin could only be detected at the spheroid surface, displaying patches of varying size and not constituting a continuous layer (Fig. 2e). On the other hand, collagen type IV was present as a largely homogeneous layer of approximately uniform thickness around the spheroid (Fig. 2f). The BM layer was found to be resistant to dissolution with mild chaotropic agents that efficiently dissolve cell-independently formed BME gels that rely on non-covalent forces for structural integrity.

To test whether the formation of the BM shell relies mainly on exogenously added BM components or on endogenous production of these proteins, correlation between shell size and the concentration of supplemented type IV collagen was investigated. Spheroids were supplemented with varying amounts of fluorescently labeled type IV collagen for the duration of spheroid/BM layer formation (24 h) and subsequently subjected to confocal fluorescence/transmittance imaging. This approach revealed that the BM thickness is strongly dependent on the concentration of exogenous type IV collagen (Fig. 3a–d). For quantitative assessment, the cross-sectional area of visualized collagen IV was assessed from a maximum fluorescence intensity projection over the full height of the spheroid and plotted versus concentration of exogenously added collagen IV. This analysis shows a direct correlation between this quantity and the concentration of supplemented collagen IV (Fig. 3e). Moreover, shell size as defined by the area in which fluorescently labeled collagen IV is present is comparable with the collagen I-devoid areas observed at the same BM-formation

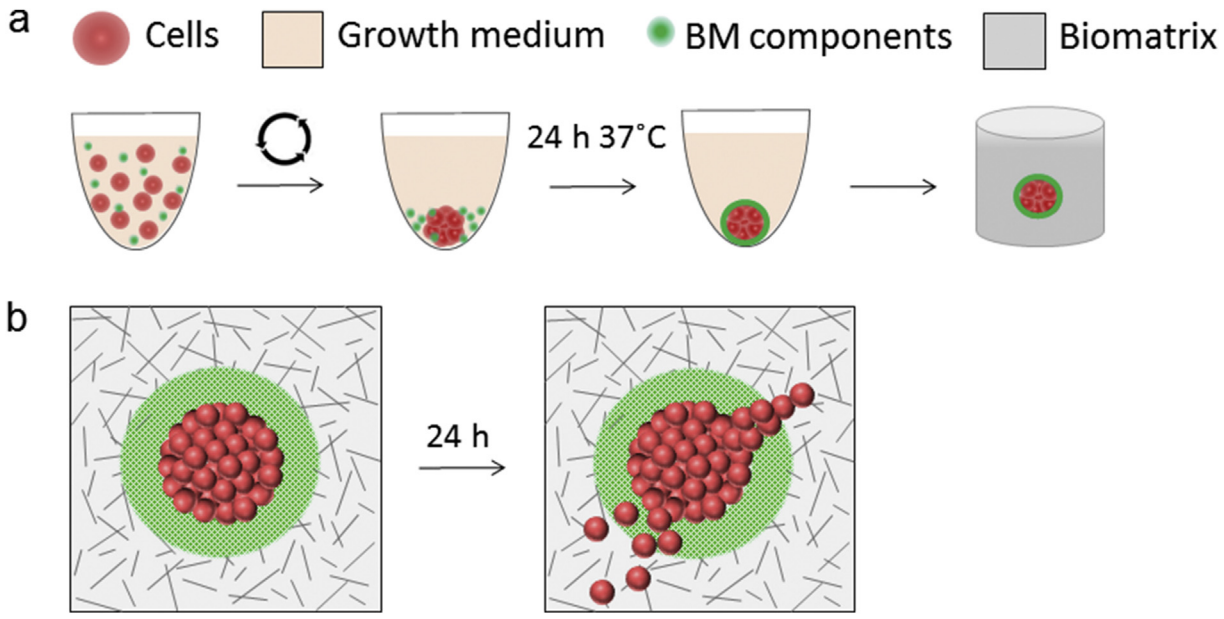

Fig. 1. Schematic representation of the experimental model used in this study. a) A multicellular tumor spheroid is produced by centrifuging cells with growth media and BM components and incubating for 24 h under low cell adhesion conditions. Spheroids fully surrounded by a BM layer are then embedded in a biopolymer solution of collagen I and/or BME that undergoes gelation. (b) Schematic depiction of transmigration of cells through the BM layer and invasion into a surrounding collagen I matrix that recapitulates initial steps of invasion in carcinomas.

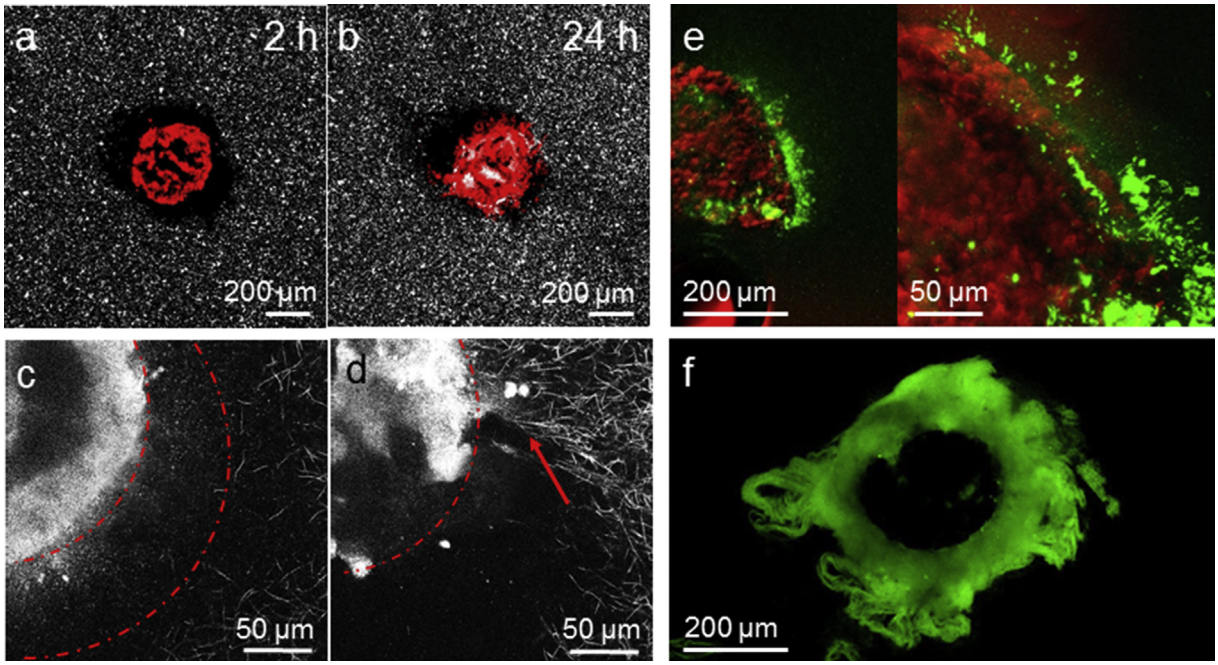

Fig. 2. Presence and composition of the basement membrane layer a, b) Confocal fluorescence (CFM) images of a representative MB468 spheroid surrounded by a BM layer at (a) 2 h and (b) 24 h post-implantation in a fluorescent bead-loaded collagen I gel. Cells are dyed with Vybrant DiD live cell-labeling solution and false colored in red, while beads appear in white. The BM layer is represented by the area free from bead and cell fluorescence. Its size and integrity change over the course of 24 h, and beads can be seen within the spheroid at that time point. Scale bar = 200 μm. c, d) Confocal reflectance (CRM) images of a representative MB468 spheroid surrounded by a BM layer and embedded in a collagen I gel (c) 2 h and (d) 24 h after embedding. At 2 h, the spheroid surface is isolated from the collagen network through the BM layer. The area devoid of collagen fibers (marked by a punctate red line) reflects the thickness of the BM. At 24 h, cell contact with collagen fibers and radial alignment of these fibers (red arrow), indicating traction generation, is evident. In (c, d), image processing software has been used to remove an optical artifact (a bright spot covering ~ 9×10^3 square pixels in the image) present in confocal reflectance images. Scale bar = 50 μm e) Representative confocal fluorescence maximum projection constructed from a z-scan over 150 μm of a shelled MB468 spheroid (red) with a BM layer containing fluorescently labeled laminin (green). Distinctive laminin accumulations at the surface of the spheroid are apparent. Scale bar = 200 μm. At right, a higher magnification maximum projection over 60 μm of a region of the spheroid is shown. Scale bar = 50 μm. f) Representative confocal fluorescence maximum projection constructed from a z-scan over 18 μm of a shelled MB468 spheroid containing fluorescently labeled type IV collagen (green) shows a dense scaffold fully surrounding the spheroid. Scale bar = 200 μm. (For interpretation of the references to colour in this figure legend, the reader is referred to the web version of this article.)

conditions in bead-exclusion experiments as shown in Fig. 2a (Fig. 3f), demonstrating that collagen IV is the main structural component of the BM shell.

Time lapse imaging revealed the time course of the shell formation process. Fluorescently labeled collagen IV accumulated around the spheroid as early as 4–5 h after process initiation. At such early time points, collagen IV was present in irregularly shaped veil-like structures emanating from the spheroid surface (Fig. S3). These structures were compacted into a denser, more uniform layer within 24 h at collagen IV concentrations 0.003–0.006 mg/ml (Fig. 3). We note that at concentrations higher than 0.006 mg/ml collagen IV, complete compaction did not always occur and irregular shell extensions sometimes remained after 24 h (data not shown). Observation of the BM structures at these early time points reveals a similar correlation between basement membrane density and size and collagen IV concentration as observed at the later time point as shown in Fig. 3. Taken together, these results indicate that the BM surrounding spheroids is primarily formed from the exogenously supplemented BM components.

We next interrogated whether the BM layer around the spheroid mimics the function and behavior of BM in vivo, where this layer separates healthy cells from the surrounding tissue – containing them within its boundary – but can be degraded and traversed by cancerous cells. To this end, spheroids with BM shells were generated from non-tumorigenic and from oncogenically transformed breast epithelial cells with the same genetic background, namely MCF10A and MCF10A-HRas cells. These spheroids were embedded into 3D collagen I matrices and monitored for the integrity of the BM layer as well as cell invasion into the collagen matrices up to 48 h after embedding. BM shell structure was visualized via confocal fluorescence microscopy of labeled type IV collagen, while spheroid architecture and cell dissemination were visualized either via transmitted light imaging or CFM following immunofluorescent staining of actin cytoskeleton. As a control, spheroids without a BM layer were used. Collagen-embedded non-cancerous MCF10A spheroids with no BM layer exhibited sheet-like expansion with a closed cell front and no individual cell invasion into the collagen (Fig. 4a). In contrast, spheroids with BM shells remained fully confined within the boundary defined by the BM throughout the monitoring period and exhibited negligible increase in spheroid cross-sectional area over 24 h (Fig. 4b); complete abrogation of cell dissemination into collagen I was effected through the introduction of the BM layer (Fig. 4c). This behavior was also observed for spheroids with a BM layer formed at the lowest collagen IV concentration yielding a complete shell (0.003 mg/ml), indicating that the presence of even the thinnest BM layer does not merely reduce but abolishes the migratory activity of MCF10A cells (Fig. S4).

In contrast to MCF10A spheroids, the oncogenically transformed MCF10A-HRas spheroids were not contained by the presence of the BM layer and exhibited multiple BM breaching events and dissemination of cells into the collagen matrix within 24 h after embedding (Fig. 5a). Compared to MCF10A-HRas spheroids with no BM layer embedded in collagen I, the density of invading cells was greatly diminished (Figs. 5a and 6a). This is consistent with the

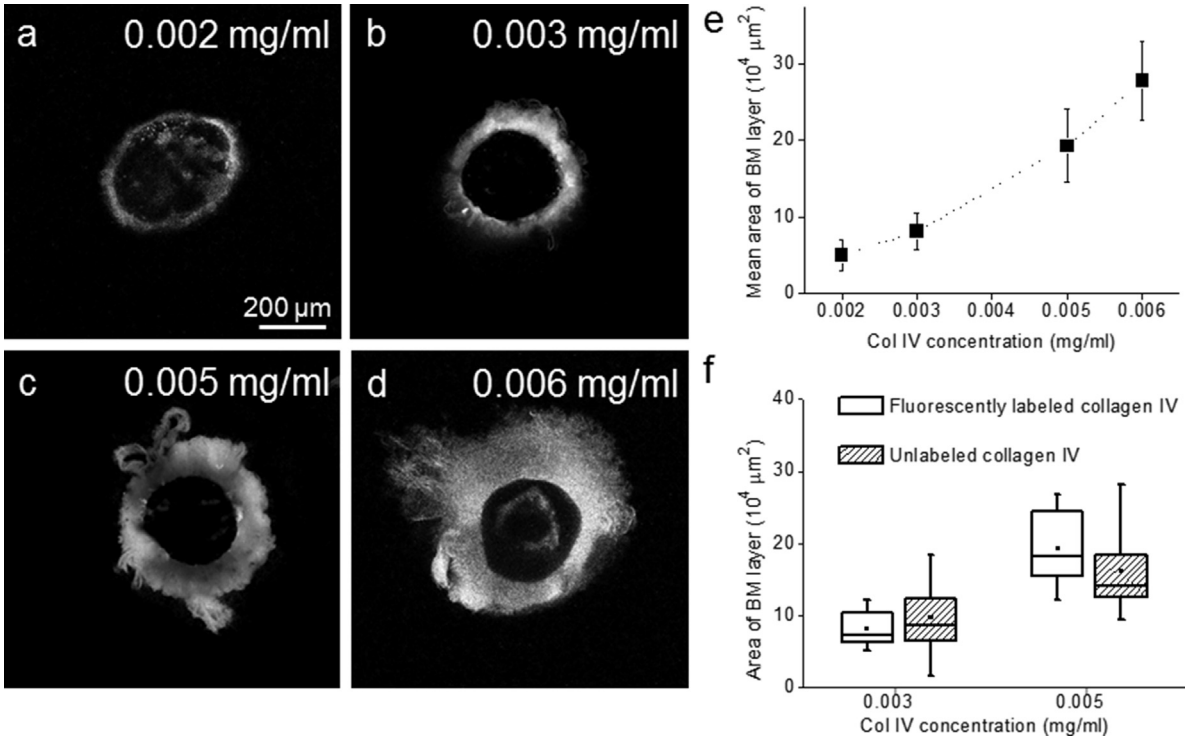

Fig. 3. BM layer thickness varies with exogenous protein concentration. a-d) Representative confocal fluorescence images of BM layers around MB468 spheroids generated with addition of (a) 0.002 mg/ml, (b) 0.003 mg/ml, (c) 0.005 mg/ml, and (d) 0.006 mg/ml collagen IV. Images are maximum projections over 30 μm centered at the spheroid midpoint axially. Images show spheroids 1 h after implantation into collagen. Scale bar = 200 μm. e) Quantification of BM cross-sectional area as a function of exogenous collagen IV concentration demonstrates correlation between these quantities. For this analysis, the area of the spheroid derived from transmitted light images was subtracted from the area of the respective BM shell derived from confocal fluorescence maximum projections. Mean values ± SD are shown, sample number n ≥ 7 for every condition. f) Comparative analysis of the area of BM shells as derived from collagen IV fluorescence (as in Fig. 3a–d) and as derived from fluorescent bead exclusion area (as in Fig. 2a) demonstrates that the collagen IV-positive scaffold has a comparable thickness at a given collagen IV concentration to that of the total BM shell. Box plots show first to third quartiles with median denoted by a line and mean with a symbol; whiskers show minimal and maximal values, sample number n ≥ 10 for every condition.

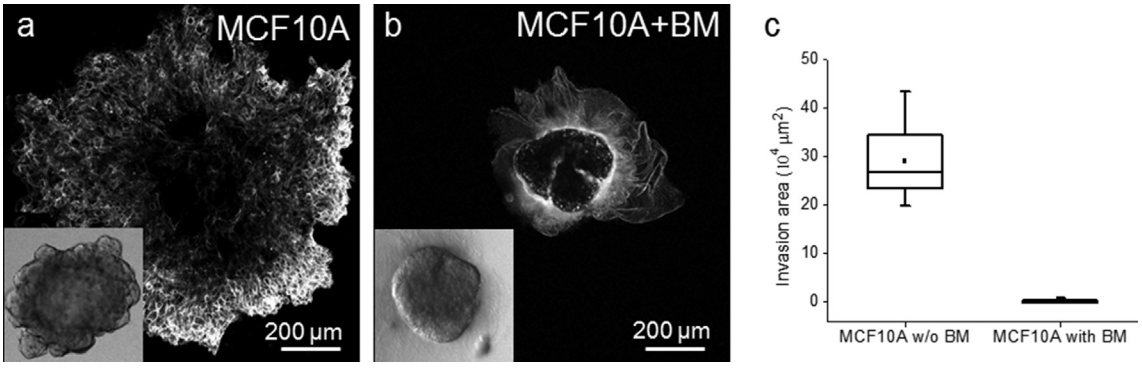

Fig. 4. Non-cancerous MCF10A cells do not breach the BM layer. a) Representative confocal fluorescence maximum projection of a phalloidin-stained MCF10A MTS 24 h after embedding in a 3D collagen matrix depicts sheet-like expansion and spreading of the spheroid into the matrix. Scale bar = 200 μm. Inset in the left corner shows a transmitted light image of this spheroid 1 h after implantation into collagen. b) Representative confocal fluorescence maximum projection of an MCF10A spheroid surrounded by a fluorescently labeled BM layer 24 h after embedding in collagen I shows complete containment of the spheroid within the BM borders. Scale bar = 200 μm. Inset shows a transmitted light image of this spheroid 1 h after implantation into collagen. c) Dependence of MCF10A spheroid invasive area on presence of the BM shell. Invasive area – defined as the difference between spheroid area at t = 2 h and t = 24 h – for MCF10A spheroids without and with a BM shell are shown in box plots depicting first to third quartiles with median denoted by a line and mean with a symbol; whiskers show minimum and maximum values. n ≥ 9 for each condition.

hypothesis that the presence of a BM layer presents a biophysical challenge for cells, which must first breach this layer before invading into the collagen I environment. Interestingly, cancer cells displayed a much higher incidence of multicellular invasion when transmigrating the BM layer, displaying streams of densely packed cells moving through the BM towards the collagen matrix, than during invasion in absence of a BM layer, where cells exclusively depicted individual mesenchymal invasion (Figs. 5b and 6a, b). The invasive streams, once in contact with the collagen I matrix, exhibited strong traction on the collagen matrix as reflected by the accumulation and high degree of alignment of collagen fibers at the tip of the invasive strand (Fig. 5c).

The combined use of collective and individual invasion modes by spheroids with a BM shell is fundamentally different from

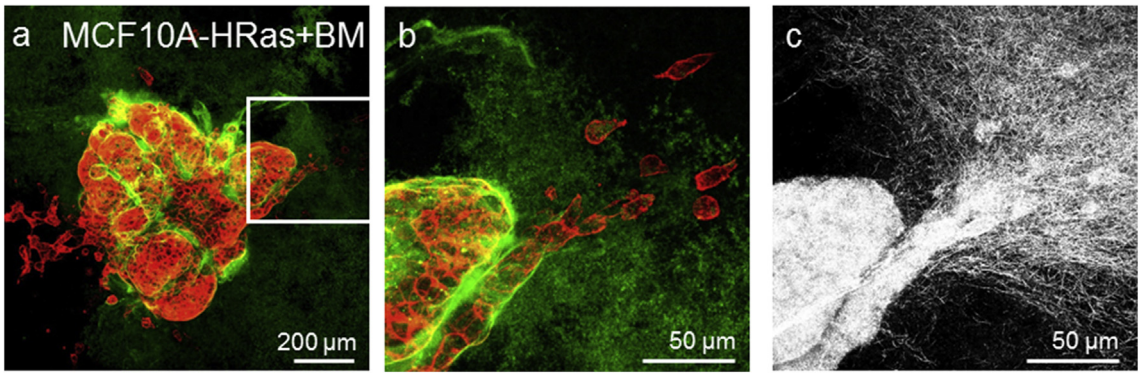

Fig. 5. Oncogenically transformed MCF10A-Ras cells effectively transmigrate the BM layer. a) Representative confocal fluorescence maximum projection of a BM-shelled phalloidin-stained MCF10A-HRas spheroid 24 h after embedding in a 3D collagen I matrix shows a combination of individual and collective invasion of cells into the surroundings. The white square defines a site of collective invasion that is shown at higher magnification in b) and c). Cells are shown in red and BM layer is shown in green. Scale bar = 200 μm. b, c) High magnification (b) confocal fluorescence and (c) reflectance maximum projections of MCF10A-Ras spheroid shown in (a). Panel (b) shows dense packing of cells during collective transmigration of the BM layer and subsequent dissemination as individual cells beyond the BM shell. Panel (c) shows extensive collagen reorganization and alignment by the multicellular invasive stream at the interface of the BM and collagen matrix. Scale bar = 50 μm. (For interpretation of the references to colour in this figure legend, the reader is referred to the web version of this article.)

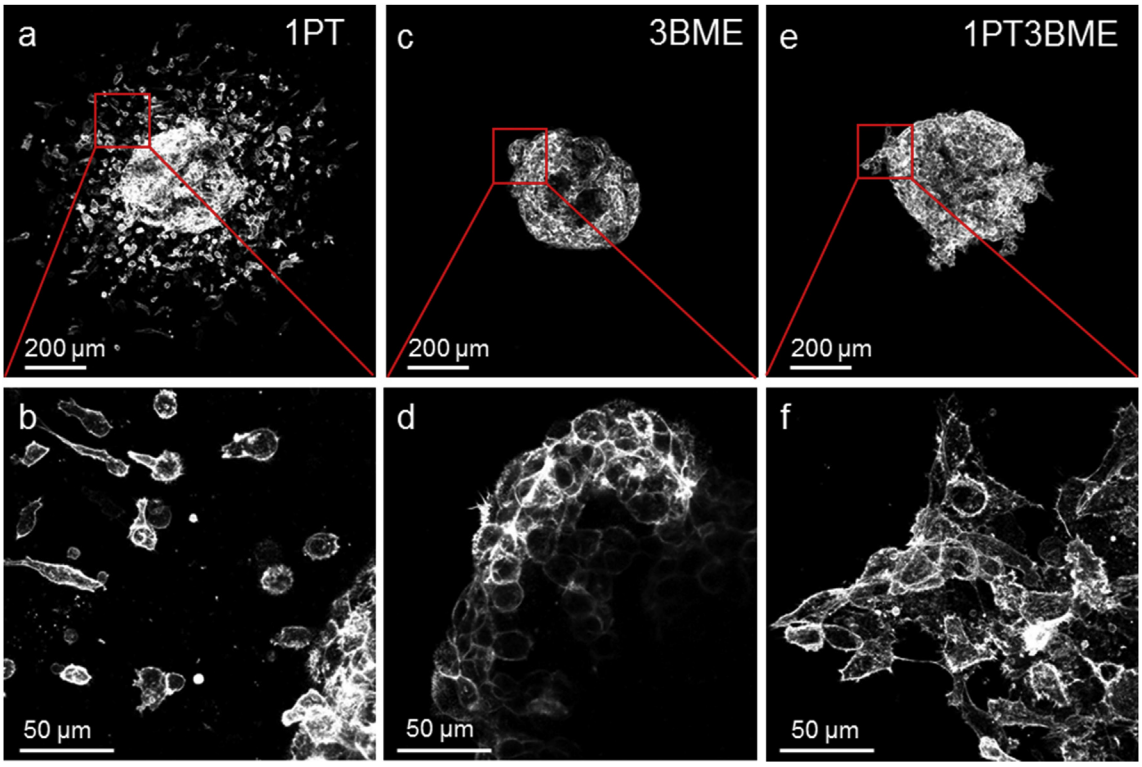

Fig. 6. MCF10A-Ras spheroids show distinct invasive modes in different matrices. a, b) Representative confocal fluorescence maximum projection of a phalloidin-stained MCF10A-HRas spheroid without a BM layer 24 h after embedding in a 3D collagen I matrix (1PT) at (a) lower and (b) higher magnification shows extensive individual invasion of cancer cells into the surroundings. Scale bar (a) = 200 μm. Scale bar (b) = 50 μm. c, d) Representative confocal fluorescence maximum projection of a phalloidin-stained MCF10A-HRas spheroid without a BM layer 24 h after embedding in a 3D BME matrix (3BME) at (c) lower and (d) higher magnification shows spherical outgrowth from the spheroid body without any cells leaving the bulk spheroid. Scale bar (c) = 200 μm. Scale bar (d) = 50 μm. e, f) Representative confocal fluorescence maximum projection of a phalloidin-stained MCF10A-HRas spheroid without a BM layer 24 h after embedding in a composite 3D collagen I/BME matrix (1PT3BME) at (e) lower and (f) higher magnification shows multicellular invasion with strongly polarized leader cells. Scale bar (e) = 200 μm. Scale bar (f) = 50 μm.

invasion observed for 3D-embedded spheroids in the absence of a BM layer. While collagen I matrices support strong individual invasion and mesenchymal cell morphology (Fig. 6a, b), a matrix composed solely of basement membrane extract (BME) does not support any invasive behavior over the assessed time scales (Fig. 6c, d). In composite collagen I/BME matrices, the cells show collective invasion as well as strong cell polarity similar to the initial migratory phenotype of shelled spheroids during invasion through the BM layer (Fig. 6e, f); however this matrix does not support the switch to individual invasion at any point.

Next, we investigated whether the observed induction of collective invasion in shelled spheroids relative to unshelled spheroids in collagen I environments is a cell-type specific response to these experimental conditions or a more general behavior of tumorigenic

cells in the presence of a BM layer. Thus, invasion studies similar to those performed on MCF10A-HRas cells were performed on cancer cells of different origin, namely MB468 breast cancer cells. MB468 spheroids prepared without a BM layer and introduced into collagen I matrices showed individual cell invasion into the surroundings, no invasion in pure BME matrices, and multicellular invasion in composite collagen I/BME matrices (Fig. S5), paralleling the invasion pattern observed in response to these matrices for MCF10A-HRas cells. When prepared with BM shells, the cells successfully traversed the BM layer and invaded into collagen (Fig. S6), as also found for MCF10A-HRas cells. While the two cancerous cell lines differ in origin, cell morphology (mesenchymal MCF10A-HRas and grape-like MB468) and time required for dissemination (24 h for MCF10A-HRas, 24–48 h for MB468), they were similar in their ability to breach and transmigrate the surrounding BM layer, in contrast to the non-tumorigenic MCF10A cells. Thus, this new experimental model recapitulates the fundamentally different physiological behavior of cancerous and non-cancerous cell aggregates surrounded by a cell-bound BM.

We next investigated molecular activity required for cells to traverse the BM layer, in particular whether matrix metalloproteinases (MMPs) were required for BM breaching and/or subsequent invasion in collagen I. To this end, MCF10A-HRas spheroids prepared with or without BM layers were pre-treated with an MMP-inhibitor cocktail targeting MMP-1, -2, -3, -7, -9 and -14 (MT1-MMP) as well as aminopeptidases and serine- and cysteine-proteases and embedded in collagen I matrices supplemented with the same inhibitors. We note that MCF10A-HRas has been reported to have upregulated expression of both MMP-2 and MMP-9, with the former regulated by MT1-MMP, relative to MCF10A [37,38]. After 24 h, samples were fixed and subjected to actin cytoskeleton staining and confocal fluorescence imaging as described earlier. It was found that the presence of the BM layer strongly modulated the cellular response to MMP inhibition. Collagen I invasion of spheroids without a BM layer was only mildly affected by MMP inhibition, with no observable differences of invasion mode or cell morphology and no significant reduction of invasive distance (Fig. 7a–c). In contrast, the invasive behavior of BM-shelled spheroids was strongly compromised by MMP inhibition. Here, the MMP inhibition led to a greater than two-fold reduction of invasion incidence (from 100% to 38.5%), as characterized by the presence of individual cancer cells in the collagen matrix, and a nearly twenty-fold reduction in the mean number of individual invasive cells (57–2.5) (Fig. 7d–f). MMP inhibition in BM-shelled spheroids did not fully prevent formation of multicellular streams, while it did completely abolish formation of invasive structures (and invasion) in BM-free spheroids embedded in composite collagen I/BME matrices, the condition that induces multicellular invasion in the absence of MMP inhibition (Fig. 7g–i). While the multicellular structures in BM-enveloped spheroids still formed under MMP inhibition, this occurred in reduced numbers per spheroid (from median 6 to 2 per spheroid). Moreover, 50% of the multicellular streams failed to breach the BM layer within 24 h, indicating that the efficiency of BM breaching is strongly dependent on MMP-mediated BM degradation. The fact that multicellular invasive streams formed under MMP inhibition in BM-enveloped spheroids while their formation was completely abrogated in bare spheroids embedded in composite matrix suggests that ECM comprising a cell-assembled non-fibrillar BM adjacent to fibrillar collagen matrix evokes a particular collective invasion mode that is more resistant to pharmacological MMP inhibition than spheroid invasion (without a BM shell) in a composite matrix consisting of a mixture of both components.

4. Discussion

Despite decades of study, the cellular events that allow an in situ circumscribed tumor to become an invasive entity and the molecular mechanisms underlying the penetration of cancer cells through the BM and adjacent ECM are not fully understood. Here, we present an optically accessible 3D model that recapitulates diverse dynamic cell-cell and cell-ECM interactions that exist as cells traverse a dense, sheet-like BM layer in advance of invasion into adjacent ECM. The experimental model presented in this study consists of spheroids containing several thousands of benign or tumorigenic cells surrounded by a BM layer and embedded into a biomechanically tunable 3D matrix (Fig. 1). Importantly, we found that non-tumorigenic cells were confined by the BM layer (Fig. 4b, Fig. S4), while spheroids composed of various cancerous cell lines breached the BM layer and invaded into the adjacent matrix within 24 h after embedding (Fig. 5, Fig. S6). This recapitulates a critical process in the progression of metastatic disease. When a dysplastic carcinoma in situ acquires the ability to traverse the BM, the lesion is classified as a malignant carcinoma [39–41]. For probing the invasive behavior of cancer cells, the model presented here is superior to embedding spheroids in pure collagen I matrices, as some non-cancerous epithelial cells spread from the spheroid in 3D collagen I matrices despite their benign character (Fig. 4a). While the cells maintain tight cell-cell contacts and a closed cell front more reminiscent of sheet expansion than true invasion in a collagen matrix, the spheroid – in absence of a BM layer – loses its original architecture and does not fully reflect its non-tumorigenic nature. This is avoided by surrounding the MTS with a dense layer of BM (compare Fig. 4a and b).

While many models suggest metastasis begins with individual cells undergoing the epithelial-mesenchymal transition (EMT) and leaving the boundaries of the primary tumor, analysis of tumor-stroma interfaces in clinical samples has revealed that it is the presence of invasive cell clusters [42], also termed tumor buds, that correlates with metastatic progression and poor prognosis in various solid tumor types [43–47]. This highlights the importance of understanding the cellular and molecular underpinnings of collective cancer cell invasion and the need for physiologically relevant in vitro models supporting this crucial mode of invasion. To date, in vitro settings for the study of collective cancer cell migration have relied primarily on 2D scratch/wound assays or on assays using spheroids or organoids embedded in 3D matrices, typically composed of collagen I or BME [48–52]. We and others have reported differential invasive behavior for cancerous cells in fibrillar (collagen I) vs. non-fibrillar (BME) 3D matrices, with collagen I typically being more supportive of invasion than is non-fibrillar BME, which did not lead to invasion in either spheroids or organoids of known tumorigenic breast, ovarian and prostate cancer cells [27,52–54]. Recently, we demonstrated that one breast cancer cell line showed individual invasion in collagen I matrices, no invasion in BME, and a primarily collective mode of invasion in a composite collagen I/BME matrix [27]. These results mirror those found in the MCF10A-HRas and MB468 cell lines shown here (Fig. 6, Fig. S5). Although the composite matrix appears to be a better system to evoke and study collective invasion than do homogeneous collagen I or BME matrices, a homogeneous environment does not recapitulate the in vivo setting in which cells are faced with distinct ECM components serially, as epithelial based tumors must first breach a cell-bound BM layer to subsequently migrate through stromal ECM.

Thus, the presence of the BM-ECM interface and the structure of the BM layer, which is intimately related to the mechanism of its generation, are a critical advantage of the shelled spheroid system described here. Conventional assays probing cell invasion in BM

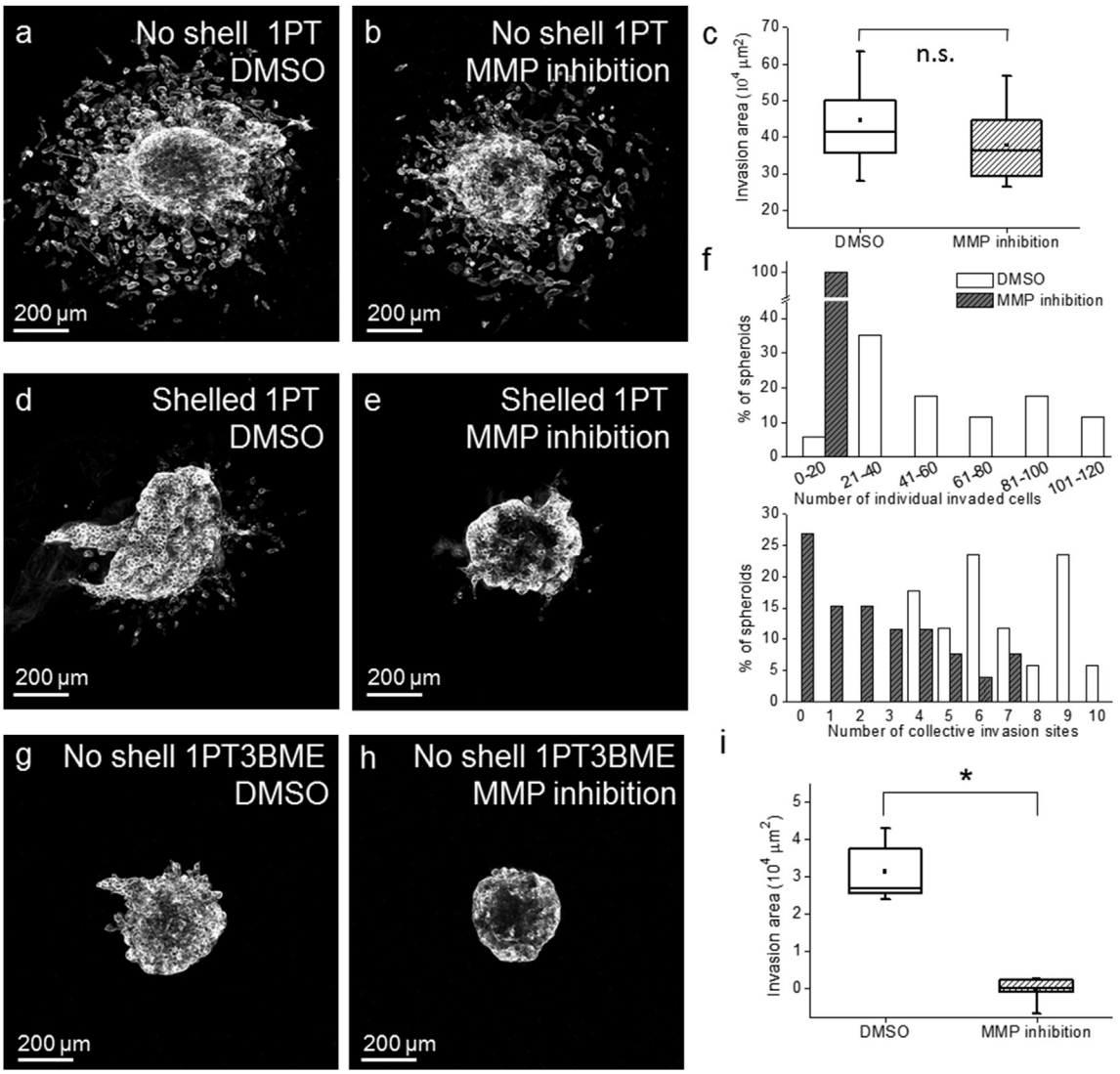

Fig. 7. Differential effects of MMP inhibition as a function of ECM. a, b) Representative confocal fluorescence maximum projections of (a) solvent control and (b) MMP inhibitor-treated phalloidin-stained MCF10A-HRas spheroids without a BM layer 24 h after embedding in a 3D collagen I matrix. Scale bar = 200 µm. c) Quantitative analysis of MCF10A-HRas spheroid invasion in collagen I under MMP inhibition reveals no significant difference ($p < 0.05$) in invasive distance between the treated and control groups. Invasive distances are shown with box plots depicting first to third quartiles with median denoted by a line and mean with a symbol; whiskers show minimum and maximum values, sample number $n \geq 12$ for every condition. d, e) Representative confocal fluorescence maximum projections of (d) solvent control and (e) MMP inhibitor-treated phalloidin-stained MCF10A-HRas spheroids with a BM layer 24 h after embedding in a 3D collagen I matrix. Scale bar = 200 µm. f) Quantitative analysis of BM-shelled MCF10A-HRas spheroid invasion in collagen I under MMP inhibition reveals significant differences in number of collective invasion sites and number of individual cells invaded in the collagen matrix per spheroid with $p < 0.05$ obtained in the non-parametrical Mann-Whitney test. Histograms show the percentage of spheroids with stated number of collective invasion sites or individual invaded cells in the inhibitor-treated versus the control group. $n \geq 17$ for every condition. g, h) Representative confocal fluorescence maximum projections of (g) solvent control and (h) MMP inhibitor-treated phalloidin-stained MCF10A-HRas spheroids without a BM layer 24 h after embedding in a composite collagen I/BME matrix show abrogation of invasion under MMP inhibition. Scale bar = 200 µm. i) Quantitative analysis of MCF10A-HRas spheroid invasion in composite collagen I/BME matrix under MMP inhibition reveals significant difference in invasive area between the treated and control groups, with $p < 0.05$ obtained in the Mann-Whitney test. Invasive areas for inhibitor and control groups are shown with box plots depicting first to third quartiles with median denoted by a line and mean with a symbol; whiskers show minimum and maximum values, sample number $n \geq 6$ for every condition.

commonly use basement membrane extract polymerized in a cell-independent manner. In contrast, in the shelled spheroid protocol presented here, the BM layer is assembled from supplemented components in a cell-mediated process. This process requires functional β1 integrin receptors since antibody-mediated β1 integrin inhibition strongly compromised the formation of a continuous and dense BM layer (data not shown). This is in accordance with the β1 integrin-dependent mechanism reported for BM formation in mice [55] and suggests that the formation of the BM layer in the presented experimental system requires similar cellular mechanisms to the respective process in vivo. This hypothesis is supported by the observation that in the shelled spheroid model presented here, laminin is bound and forms a thin patchy layer directly at the spheroid surface (Fig. 2e) while collagen IV is polymerized into a complex network that constitutes the bulk of the BM structure (Figs. 2f and 3). This closely recapitulates the reported molecular mechanisms of BM assembly in vivo, where laminin is polymerized at the cell surface and serves as the initial template for scaffold formation through type IV collagen polymerization [56,57].

BME polymerized in a cell-independent manner is not only more compliant than endogenous BM [58,59], it also lacks some hallmarks of mature BM structure, such as covalently cross-linked collagen IV [53,60,61]. Cells thus may use distinct invasion strategies in traversing BME relative to those used in cell-assembled BM

in vivo or in the shelled spheroid model presented here. This hypothesis is supported by our finding that cancer cells that are non-invasive in 3D BME gels can efficiently transmigrate the BM layer in the presented model (compare Figs. 5a and 6c, Figs. S5b and S6). This finding is also consistent with studies showing that matrix stiffness and architecture determine cancer cell invasion efficiency and strategy and regulate dynamic switching between invasive modes, such as mesenchymal and amoeboid invasion [27,62–64]. For individually invading cancer cells, some 3D environments preferentially induce mesenchymal invasion requiring cell–matrix adhesion and MMP-mediated ECM proteolysis, while others induce migratory modes relying on ROCK-mediated cortical actomyosin contractility, such as MMP-dependent lobopodial migration and MMP-independent amoeboid migration [64,65]. For collective invasion, mechanistically distinct invasive modes have not been as well-characterized. Indeed, the biomechanical determinants (such as matrix stiffness and porosity) and cellular determinants (such as cell contractility and adhesion and protease requirements) of collective invasion modes are yet to be fully elucidated. For example, it is possible that the existence of a confining BM shell around a growing spheroid may drive collective invasion by generating elevated pressure within the spheroid that mimics the high interstitial pressure observed in solid tumors, a characteristic that has been linked to altered migratory behavior in vitro and increased metastasis and poor prognosis in vivo [66–69].

Interestingly, we find that in MCF10A-HRas spheroids surrounded by a layer of cell-assembled BM, the formation of multicellular streams and a degree of successful invasion occurs under MMP inhibition targeting both secreted MMPs and the membrane-bound MT1-MMP. In contrast, this cellular behavior is completely abolished in unshelled spheroids embedded in composite matrices (Fig. 7). The lower sensitivity to MMP inhibition suggests that the cells utilize different invasion mechanisms during transmigration of cell-assembled BM than when confronted with BME polymerized in a cell-independent manner. A study utilizing decellularized peritoneal BM demonstrated that transmigration of native ex vivo BM has different requirements for MMP activity, relying exclusively on membrane-bound MMPs (MT1-3 MMPs) than invasion of in vitro reconstituted BME that utilized secreted MMPs [61]. Thus, it is particularly important to address the mechanisms of BM breaching in a system that not only recapitulates the biochemical composition of BM but also more closely resembles its biomechanical properties in vivo. Whether the multicellular invasion mode seen in this study uses membrane-bound MMPs (such as MT2- or MT3-MMP) that were not specifically targeted by the protease inhibitors used here or whether the cell-assembled BM provides mechano-transductory stimuli inducing a less MMP-dependent collective invasion mode remains to be clarified. However, our finding of limited MMP dependence in the shelled spheroid model, together with the largely MMP-independent migratory mode of individual cancer cells in fibrillar collagen I matrix, offers an explanation for the inefficiency of MMP inhibition as a treatment strategy for late stage cancers [70].

5. Conclusion

We have developed a novel experimental model in which tumor spheroids surrounded by a cell-bound BM of tunable thickness are generated and may be subsequently embedded in a second biopolymer matrix such that the cells serially encounter multiple, adjacent extracellular environments. Using this model, central initial events of metastatic progression were recapitulated in a physiologically relevant setting. First, we showed that tumorigenic breast cancer cell lines of two different subtypes can breach this BM within 24 h, while non-cancerous breast epithelial cells were fully retained within BM borders, thus reproducing an early hallmark of metastatic behavior. We also demonstrated selective cancer cell utilization of collective migration for transmigration of the physically challenging BM layer. Moreover, this study revealed that while BM breaching, in contrast to collagen I invasion, is an MMP-dependent process, it is less susceptible to pharmacological MMP inhibition then collective invasion in homogeneous composite matrices and cannot be fully abolished by such. Thus, we showed that the heterogeneous environment comprising a distinct non-fibrillar BM and an adjacent fibrillar ECM evoked a complex invasive phenotype that differed from any homogeneous ECM condition tested and that the described model represents a physiologically highly relevant setting for addressing cellular characteristics and treatment responses in metastasizing solid tumors.

Acknowledgements

This work was supported in part by the National Science Foundation and the National Institutes of Health via PESO 1227297.

Appendix A. Supplementary data

Supplementary data related to this article can be found at http://dx.doi.org/10.1016/j.biomaterials.2016.11.014.

References

[1] S. Valastyan, R.A. Weinberg, Tumor metastasis: molecular insights and evolving paradigms, Cell 147 (2011) 275–292.
[2] S. Kumar, V.M. Weaver, Mechanics, malignancy, and metastasis: the force journey of a tumor cell, Cancer Metastasis Rev. 28 (2009) 113–127.
[3] P. Lu, V.M. Weaver, Z. Werb, The extracellular matrix: a dynamic niche in cancer progression, J. Cell Biol. 196 (2012) 395–406.
[4] R. Kalluri, Basement membranes: structure, assembly and role in tumour angiogenesis, Nat. Rev. Cancer 3 (2003) 422–433.
[5] P.D. Yurchenco, Basement membranes: cell scaffoldings and signaling platforms, Cold Spring Harb. Perspect. Biol. 3 (2011).
[6] L.A. Liotta, K. Tryggvason, S. Garbisa, I. Hart, C.M. Foltz, S. Shafie, Metastatic potential correlates with enzymatic degradation of basement membrane collagen, Nature 284 (1980) 67–68.
[7] A. Martinez-Hernandez, P.S. Amenta, The basement membrane in pathology, Lab. Investig. 48 (1983) 656–677.
[8] J.V. Frei, The fine structure of the basement membrane in epidermal tumors, J. Cell Biol. 15 (1962) 335–342.
[9] F.T. Bosman, M. Havenith, J.P. Cleutjens, Basement membranes in cancer, Ultrastruct. Pathol. 8 (1985) 291–304.
[10] S. Spaderna, O. Schmalhofer, F. Hlubek, G. Berx, A. Eger, S. Merkel, et al., A transient, EMT-linked loss of basement membranes indicates metastasis and poor survival in colorectal cancer, Gastroenterology 131 (2006) 830–840.
[11] A. Bergamaschi, E. Tagliabue, T. Sorlie, B. Naume, T. Triulzi, R. Orlandi, et al., Extracellular matrix signature identifies breast cancer subgroups with different clinical outcome, J. Pathol. 214 (2008) 357–367.
[12] K. Polyak, Molecular markers for the diagnosis and management of ductal carcinoma in situ, J. Natl. Cancer Inst. Monogr. 2010 (2010) 210–213.
[13] J.K. Mouw, G. Ou, V.M. Weaver, Extracellular matrix assembly: a multiscale deconstruction, Nat. Rev. Mol. Cell Biol. 15 (2014) 771–785.
[14] G.G. Zhu, L. Risteli, M. Makinen, J. Risteli, A. Kauppila, F. Stenback, Immunohistochemical study of type I collagen and type I pN-collagen in benign and malignant ovarian neoplasms, Cancer 75 (1995) 1010–1017.
[15] S. Kauppila, F. Stenback, J. Risteli, A. Jukkola, L. Risteli, Aberrant type I and type III collagen gene expression in human breast cancer in vivo, J. Pathol. 186 (1998) 262–268.
[16] I.J. Huijbers, M. Iravani, S. Popov, D. Robertson, S. Al-Sarraj, C. Jones, et al., A role for fibrillar collagen deposition and the collagen internalization receptor endo180 in glioma invasion, PLoS One 5 (2010) e9808.
[17] S. Alowami, S. Troup, S. Al-Haddad, I. Kirkpatrick, P.H. Watson, Mammographic density is related to stroma and stromal proteoglycan expression, Breast Cancer Res. 5 (2003) R129–R135.
[18] Y.P. Guo, L.J. Martin, W. Hanna, D. Banerjee, N. Miller, E. Fishell, et al., Growth factors and stromal matrix proteins associated with mammographic densities, Cancer Epidemiol. Biomarker. Prev. 10 (2001) 243–248.
[19] P.P. Provenzano, K.W. Eliceiri, J.M. Campbell, D.R. Inman, J.G. White, P.J. Keely, Collagen reorganization at the tumor-stromal interface facilitates local invasion, BMC Med. 4 (2006) 38.
[20] M.W. Conklin, J.C. Eickhoff, K.M. Riching, C.A. Pehlke, K.W. Eliceiri,

P.P. Provenzano, et al., Aligned collagen is a prognostic signature for survival in human breast carcinoma, Am. J. Pathol. 178 (2011) 1221–1232.
[21] R. Kalluri, R.A. Weinberg, The basics of epithelial-mesenchymal transition, J. Clin. Investig. 119 (2009) 1420–1428.
[22] S. Gurzu, S. Turdean, A. Kovecsi, A.O. Contac, I. Jung, Epithelial-mesenchymal, mesenchymal-epithelial, and endothelial-mesenchymal transitions in malignant tumors: an update, World J. Clin. Cases 3 (2015) 393–404.
[23] J.L. Leight, M.A. Wozniak, S. Chen, M.L. Lynch, C.S. Chen, Matrix rigidity regulates a switch between TGF-beta1-induced apoptosis and epithelial-mesenchymal transition, Mol. Biol. Cell 23 (2012) 781–791.
[24] S.C. Wei, L. Fattet, J.H. Tsai, Y. Guo, V.H. Pai, H.E. Majeski, et al., Matrix stiffness drives epithelial-mesenchymal transition and tumour metastasis through a TWIST1-G3BP2 mechanotransduction pathway, Nat. Cell Biol. 17 (2015) 678–688.
[25] K.R. Levental, H. Yu, L. Kass, J.N. Lakins, M. Egeblad, J.T. Erler, et al., Matrix crosslinking forces tumor progression by enhancing integrin signaling, Cell 139 (2009) 891–906.
[26] N.R. Lang, K. Skodzek, S. Hurst, A. Mainka, J. Steinwachs, J. Schneider, et al., Biphasic response of cell invasion to matrix stiffness in three-dimensional biopolymer networks, Acta Biomater. 13 (2015) 61–67.
[27] A. Guzman, M.J. Ziperstein, L.J. Kaufman, The effect of fibrillar matrix architecture on tumor cell invasion of physically challenging environments, Biomaterials 35 (2014) 6954–6963.
[28] J. Condeelis, J.E. Segall, Intravital imaging of cell movement in tumours, Nat. Rev. Cancer 3 (2003) 921–930.
[29] S.I. Ellenbroek, J. van Rheenen, Imaging hallmarks of cancer in living mice, Nat. Rev. Cancer 14 (2014) 406–418.
[30] C.R. Thoma, M. Zimmermann, I. Agarkova, J.M. Kelm, W. Krek, 3D cell culture systems modeling tumor growth determinants in cancer target discovery, Adv. Drug Deliv. Rev. 69–70 (2014) 29–41.
[31] E. Katz, S. Dubois-Marshall, A.H. Sims, P. Gautier, H. Caldwell, R.R. Meehan, et al., An in vitro model that recapitulates the epithelial to mesenchymal transition (EMT) in human breast cancer, PLoS One 6 (2011) e17083.
[32] M. Schoumacher, R.D. Goldman, D. Louvard, D.M. Vignjevic, Actin, microtubules, and vimentin intermediate filaments cooperate for elongation of invadopodia, J. Cell Biol. 189 (2010) 541–556.
[33] A. Ivascu, M. Kubbies, Rapid generation of single-tumor spheroids for high-throughput cell function and toxicity analysis, J. Biomol. Screen 11 (2006) 922–932.
[34] K. Wolf, I. Mazo, H. Leung, K. Engelke, U.H. von Andrian, E.I. Deryugina, et al., Compensation mechanism in tumor cell migration: mesenchymal-amoeboid transition after blocking of pericellular proteolysis, J. Cell Biol. 160 (2003) 267–277.
[35] M.P. Fay, M.A. Proschan, Wilcoxon-Mann-Whitney or t-test? On assumptions for hypothesis tests and multiple interpretations of decision rules, Stat. Surv. 4 (2010) 1–39.
[36] M.J. Ziperstein, A. Guzman, L.J. Kaufman, Breast Cancer cell line aggregate morphology does not predict invasive capacity, PLoS One 10 (2015) e0139523.
[37] A. Moon, M.S. Kim, T.G. Kim, S.H. Kim, H.E. Kim, Y.Q. Chen, et al., H-ras, but not N-ras, induces an invasive phenotype in human breast epithelial cells: a role for MMP-2 in the H-ras-induced invasive phenotype, Int. J. Cancer 85 (2000) 176–181.
[38] D. Al-Raawi, H. Abu-El-Zahab, M. El-Shinawi, M.M. Mohamed, Membrane type-1 matrix metalloproteinase (MT1-MMP) correlates with the expression and activation of matrix metalloproteinase-2 (MMP-2) in inflammatory breast cancer, Int. J. Clin. Exp. Med. 4 (2011) 265–275.
[39] D. Hanahan, R.A. Weinberg, The hallmarks of cancer, Cell 100 (2000) 57–70.
[40] R.G. Rowe, S.J. Weiss, Breaching the basement membrane: who, when and how? Trends Cell Biol. 18 (2008) 560–574.
[41] F.T. Bosman, The borderline: basement membranes and the transition from premalignant to malignant neoplasia, Microsc. Res. Tech. 28 (1994) 216–225.
[42] D. Hanahan, R.A. Weinberg, Hallmarks of cancer: the next generation, Cell 144 (2011) 646–674.
[43] N. Ohike, I. Coban, G.E. Kim, O. Basturk, T. Tajiri, A. Krasinskas, et al., Tumor budding as a strong prognostic indicator in invasive ampullary adenocarcinomas, Am. J. Surg. Pathol. 34 (2010) 1417–1424.
[44] B. Mitrovic, D.F. Schaeffer, R.H. Riddell, R. Kirsch, Tumor budding in colorectal carcinoma: time to take notice, Mod. Pathol. 25 (2012) 1315–1325.
[45] E. Karamitopoulou, I. Zlobec, B. Gloor, A. Kondi-Pafiti, A. Lugli, A. Perren, Loss of Raf-1 kinase inhibitor protein (RKIP) is strongly associated with high-grade tumor budding and correlates with an aggressive phenotype in pancreatic ductal adenocarcinoma (PDAC), J. Transl. Med. 11 (2013) 311.
[46] F. Liang, W. Cao, Y. Wang, L. Li, G. Zhang, Z. Wang, The prognostic value of tumor budding in invasive breast cancer, Pathol. Res. Pract. 209 (2013) 269–275.
[47] Y. Sun, F. Liang, W. Cao, K. Wang, J. He, H. Wang, et al., Prognostic value of poorly differentiated clusters in invasive breast cancer, World J. Surg. Oncol. 12 (2014) 310.
[48] T. Das, K. Safferling, S. Rausch, N. Grabe, H. Boehm, J.P. Spatz, A molecular mechanotransduction pathway regulates collective migration of epithelial cells, Nat. Cell Biol. 17 (2015) 276–287.
[49] M.L. Graves, J.A. Cipollone, P. Austin, E.M. Bell, J.S. Nielsen, C.B. Gilks, et al., The cell surface mucin podocalyxin regulates collective breast tumor budding, Breast Cancer Res. 18 (2016) 11.
[50] L.J. Kaufman, C.P. Brangwynne, K.E. Kasza, E. Filippidi, V.D. Gordon, T.S. Deisboeck, et al., Glioma expansion in collagen I matrices: analyzing collagen concentration-dependent growth and motility patterns, Biophys. J. 89 (2005) 635–650.
[51] Y.L. Yang, S. Motte, L.J. Kaufman, Pore size variable type I collagen gels and their interaction with glioma cells, Biomaterials 31 (2010) 5678–5688.
[52] K.V. Nguyen-Ngoc, K.J. Cheung, A. Brenot, E.R. Shamir, R.S. Gray, W.C. Hines, et al., ECM microenvironment regulates collective migration and local dissemination in normal and malignant mammary epithelium, Proc. Natl. Acad. Sci. U. S. A. 109 (2012) E2595–E2604.
[53] K.L. Sodek, T.J. Brown, M.J. Ringuette, Collagen I but not Matrigel matrices provide an MMP-dependent barrier to ovarian cancer cell penetration, BMC Cancer 8 (2008) 223.
[54] V. Harma, J. Virtanen, R. Makela, A. Happonen, J.P. Mpindi, M. Knuuttila, et al., A comprehensive panel of three-dimensional models for studies of prostate cancer growth, invasion and drug responses, PLoS One 5 (2010) e10431.
[55] S. Raghavan, C. Bauer, G. Mundschau, Q. Li, E. Fuchs, Conditional ablation of beta1 integrin in skin. Severe defects in epidermal proliferation, basement membrane formation, and hair follicle invagination, J. Cell Biol. 150 (2000) 1149–1160.
[56] K.K. McKee, D. Harrison, S. Capizzi, P.D. Yurchenco, Role of laminin terminal globular domains in basement membrane assembly, J. Biol. Chem. 282 (2007) 21437–21447.
[57] S. Li, P. Liquari, K.K. McKee, D. Harrison, R. Patel, S. Lee, et al., Laminin-sulfatide binding initiates basement membrane assembly and enables receptor signaling in Schwann cells and fibroblasts, J. Cell Biol. 169 (2005) 179–189.
[58] S.S. Soofi, J.A. Last, S.J. Liliensiek, P.F. Nealey, C.J. Murphy, The elastic modulus of Matrigel as determined by atomic force microscopy, J. Struct. Biol. 167 (2009) 216–219.
[59] W. Halfter, P. Oertle, C.A. Monnier, L. Camenzind, M. Reyes-Lua, H. Hu, et al., New concepts in basement membrane biology, FEBS J. 282 (2015) 4466–4479.
[60] S. Even-Ram, K.M. Yamada, Cell migration in 3D matrix, Curr. Opin. Cell Biol. 17 (2005) 524–532.
[61] K. Hotary, X.Y. Li, E. Allen, S.L. Stevens, S.J. Weiss, A cancer cell metalloprotease triad regulates the basement membrane transmigration program, Genes Dev. 20 (2006) 2673–2686.
[62] K. Wolf, M. Te Lindert, M. Krause, S. Alexander, J. Te Riet, A.L. Willis, et al., Physical limits of cell migration: control by ECM space and nuclear deformation and tuning by proteolysis and traction force, J. Cell Biol. 201 (2013) 1069–1084.
[63] M.H. Zaman, L.M. Trapani, A.L. Sieminski, D. Mackellar, H. Gong, R.D. Kamm, et al., Migration of tumor cells in 3D matrices is governed by matrix stiffness along with cell-matrix adhesion and proteolysis, Proc. Natl. Acad. Sci. U. S. A. 103 (2006) 10889–10894.
[64] R.J. Petrie, N. Gavara, R.S. Chadwick, K.M. Yamada, Nonpolarized signaling reveals two distinct modes of 3D cell migration, J. Cell. Biol. 197 (2012) 439–455.
[65] V. Sanz-Moreno, C.J. Marshall, The plasticity of cytoskeletal dynamics underlying neoplastic cell migration, Curr. Opin. Cell Biol. 22 (2010) 690–696.
[66] J.M. Tse, G. Cheng, J.A. Tyrrell, S.A. Wilcox-Adelman, Y. Boucher, R.K. Jain, et al., Mechanical compression drives cancer cells toward invasive phenotype, Proc. Natl. Acad. Sci. U. S. A. (2012) 911–916.
[67] M. Milosevic, A. Fyles, D. Hedley, M. Pintilie, W. Levin, L. Manchul, et al., Interstitial fluid pressure predicts survival in patients with cervix cancer independent of clinical prognostic factors and tumor oxygen measurements, Cancer Res. 61 (2001) 6400–6405.
[68] T. Hompland, C. Ellingsen, K.M. Ovrebo, E.K. Rofstad, Interstitial fluid pressure and associated lymph node metastasis revealed in tumors by dynamic contrast-enhanced MRI, Cancer Res. 72 (2012) 4899–4908.
[69] W.J. Polacheck, A.E. German, A. Mammoto, D.E. Ingber, R.D. Kamm, Mechanotransduction of fluid stresses governs 3D cell migration, Proc. Natl. Acad. Sci. U. S. A. 111 (2014) 2447–2452.
[70] L.M. Coussens, B. Fingleton, L.M. Matrisian, Matrix metalloproteinase inhibitors and cancer: trials and tribulations, Science 295 (2002) 2387–2392.